

Magnetic field dynamos and magnetically triggered flow instabilities

F Stefani¹, T Albrecht², R Arlt³, M Christen⁴, A Gailitis⁵, M Gellert³, A Giesecke¹, O Goepfert⁶, J Herault⁷, O N Kirillov⁸, G. Mamatsashvili¹, J Priede⁹, G Rüdiger³, M Seilmayer¹, A Tilgner⁶ and T Vogt¹

¹ Helmholtz-Zentrum Dresden – Rossendorf, Bautzner Landstraße 400, D-01328 Dresden, Germany

² Department of Mechanical and Aerospace Engineering, Monash University, VIC 3800, Australia

³ Leibniz-Institut für Astrophysik Potsdam, An der Sternwarte 16, D-14482 Potsdam, Germany

⁴ Technische Universität Dresden, Institut für Energietechnik, D-01062 Dresden, Germany

⁵ Institute of Physics, University of Latvia, LV-2169 Salaspils, Miera iela 32, Latvia

⁶ Institute of Geophysics, University of Göttingen, Friedrich-Hund-Platz 1, D-37077 Göttingen, Germany

⁷ Laboratoire des Sciences du Numérique de Nantes (LS2N), CNRS, IMT Atlantique, Nantes, France

⁸ Northumbria University, Mathematics, Physics and Electrical Engineering, Ellison Building, D219 Newcastle upon Tyne NE1 8ST, United Kingdom

⁹ Flow Measurement Research Centre, Coventry University, UK

E-mail: F.Stefani@hzdr.de

Abstract. The project A2 of the LIMTECH Alliance aimed at a better understanding of those magnetohydrodynamic instabilities that are relevant for the generation and the action of cosmic magnetic fields. These comprise the hydromagnetic dynamo effect and various magnetically triggered flow instabilities, such as the magnetorotational instability and the Tayler instability. The project was intended to support the experimental capabilities to become available in the framework of the DREsden Sodium facility for DYNamo and thermohydraulic studies (DRESDYN). An associated starting grant was focused on the dimensioning of a liquid metal experiment on the newly found magnetic destabilization of rotating flows with positive shear. In this paper, the main results of these two projects are summarized.

1. Introduction

Magnetic fields of planets, stars and galaxies are generated by the homogeneous dynamo effect [1, 2, 3]. Once produced, cosmic magnetic fields can play a surprisingly active role in cosmic structure formation via various magnetically triggered flow instabilities, such as the celebrated magnetorotational instability (MRI) [4] and the current-driven Tayler instability (TI) [5].

Complementary to the decades-long theoretical and numerical efforts to understand these fundamental magnetohydrodynamic effects, the last years have seen great progress in dedicated experimental investigations [6, 7, 8]. After the pioneering Riga and Karlsruhe dynamo

experiments [9, 10, 11], it was in particular the rich dynamics observed in the French von Kármán Sodium (VKS) experiment [12] that provoked much interest throughout the dynamo community. The observed reversals, excursions, bursts, hemispherical fields etc. inspired new activities to understand the essential physics behind the corresponding planetary phenomena [13, 14, 15, 16].

For magnetically triggered flow instabilities, the situation is more subtle. Interesting results had been obtained in a liquid sodium spherical Couette experiment in Maryland in form of coherent velocity/magnetic field fluctuations showing up in a parameter region reminiscent of MRI [17], as well as in the GaInSn Taylor-Couette (TC) experiment in Princeton which provided evidence for slow magneto-Coriolis waves [18] and a free-Shercliff layer instability [19]. Despite these achievements, both experiments have corroborated the intricacies of demonstrating the standard version of MRI (SMRI) for which a purely axial field is applied. For liquid metal TC flows, in particular, the complications result from the compromising effect of axial boundaries on the flow structure at those high Reynolds numbers ($> 10^6$) that are necessary if magnetic Reynolds numbers of order 10 are required.

More conclusive, albeit less ambitious, was the experimental demonstration of two special types of the MRI which arise when applying helical or purely azimuthal magnetic fields to the rotating flow. These instabilities have been coined helical MRI (HMRI) and azimuthal MRI (AMRI), respectively. As was first shown by Hollerbach and Rüdiger [20], the essentially inductionless, axisymmetric ($m = 0$) HMRI scales with the Reynolds and Hartmann number rather than with magnetic Reynolds and Lundquist number as SMRI with which it is monotonically connected, though [20, 21]. It is this scaling behaviour which makes experimental investigations of HMRI much easier than those of SMRI. Indeed, first evidence of HMRI occurring in the predicted parameter regions of Hartmann number with roughly correct eigenfrequencies was demonstrated in the PROMISE experiment at Helmholtz-Zentrum Dresden-Rossendorf (HZDR) [22, 23]. In 2009, an improved version of this experiment - using split end-rings installed at the top and bottom of the cylinder in order to minimize the global effects of Ekman pumping - allowed to characterize HMRI by a number of parameter variations, generally in good agreement with numerical predictions [24].

Nearly at the same time, Hollerbach et al. [25] identified AMRI as a second induction-less MRI version that appears for strongly dominant azimuthal fields in form of a non-axisymmetric ($m = 1$) perturbation. When relaxing the condition, implicit for AMRI and HMRI, that the azimuthal field should be current-free in the liquid, one enters the vast field of current-driven instabilities which includes the Tayler instability (TI) [5]. This kink-type instability, whose ideal counterpart has long been known in plasma physics [26], is also discussed as a central mechanism of the non-linear Tayler-Spruit dynamo model for stellar magnetic fields [27, 28, 29]). While TI was experimentally observed prior to the start of the LIMTECH alliance [30], AMRI was first demonstrated within the funding period [31].

Despite – and partly inspired by – those experimental achievements, there are still a number of questions worth to be studied in laboratory. While realistic "bonsai" models of cosmic objects, with all dimensionless numbers matching those of planets or stars, are certainly outside the scope of laboratory feasibility [8], some new facilities still challenge the physical and technical limits of dynamo experiments. This certainly applies to the 3 m diameter spherical Couette experiment running at the University of Maryland [32, 33], to the 3 m diameter plasma dynamo experiment in Madison [34, 35], as well as to the 2 m diameter precession dynamo experiment presently under construction at HZDR [36, 37]. One of the unwelcome characteristics of these "second generation" dynamo experiments is a higher uncertainty of success. The Riga and Karlsruhe experiments were quite accurately described by kinematic dynamo codes and simplified saturation models [38, 39, 40], and even the unexpected VKS dynamo results were understood once the effect of the high permeability disks was accounted for properly

[41, 42, 43, 44]. By contrast, the outcomes of the experiments in Maryland, Madison, and Dresden are much harder to predict. In either case, this uncertainty results from the ambition to construct a truly homogeneous dynamo, which is neither driven by pumps or propellers, nor influenced by guiding blades or gradients of magnetic permeability. This higher degree of freedom makes those flows prone to exhibiting medium-size flow structures and waves, whose dynamo capabilities are still under scrutiny.

On the MRI side, the "holy grail" of observing SMRI in the lab is yet to be found. One promising set-up is the relatively flat TC experiment in Princeton which circumvents the Ekman-pumping induced distortion of the original TC flow profile by separately driving different rings of the lids. Another promising way is followed in the plasma experiment in Madison where already reasonable radial velocity profiles have been produced by a near-wall $\mathbf{j} \times \mathbf{B}$ driving of argon and helium plasmas [35]. At HZDR, a more traditional path towards SMRI is pursued: the respective experiment contains a long sodium column between two rotating cylinders exposed to a strong axial magnetic field. Yet, this axial field is complemented by an azimuthal magnetic field, which permits progressing from the well-known regime of HMRI towards the limit of SMRI by increasing the Reynolds and Hartmann number and simultaneously decreasing the ratio of azimuthal to axial field.

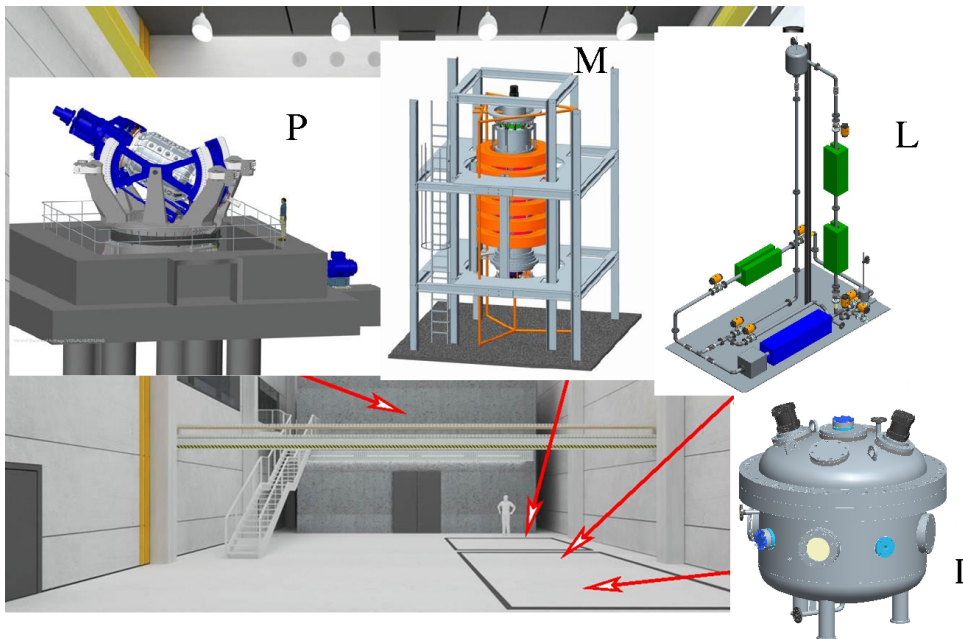


Figure 1. Interior of the central hall of the DRESHDYN facility with the main planned experiments. Precession driven dynamo experiment (P) to be installed in the containment; Taylor-Couette experiment for the investigation of the magnetorotational and the Taylor instability (M); sodium loop (L); In-Service-Inspection experiment (I). A further test stand for liquid metal batteries is also foreseen but not yet designed.

This paper summarizes research activities within the LIMTECH Alliance that were dedicated to preparations of the precession-driven dynamo experiment and the large-scale MRI experiment. Both experiments are presently under construction in frame of the DRESHDYN project at HZDR, which will include also a number of other experiments with liquid sodium (see Figure 1). On the dynamo side, activities included a number of numerical simulations of precession driven flows and their dynamo action in cylinders and cubes, as well as experimental work at a 1:6 down-

scaled water experiment. They also comprised various activities to refurbish and recommission the Riga dynamo experiment which – apart from having its own scientific goals – serves also for testing various measurement techniques for future DRESDYN experiments.

With regard to MRI/TI, the project supported the first demonstration of AMRI at the PROMISE facility at HZDR, and included theoretical and numerical work on various aspects of the interaction of rotating fluids and magnetic fields. These led to the characterization of a new magnetically triggered instability ("Super-AMRI") that destabilizes rotating flows with positive shear, to the "refutation" of Chandrasekhar's theorem for magnetized rotating flows, and to the establishment of a rigorous mathematical connection between the non-modal growth for purely hydrodynamic rotating flows and the growth rate of helical MRI.

2. Dynamos

In this section we summarize the main activities dedicated to existing and planned dynamo experiments. While the main focus was on various preparations of the DRESDYN precession driven dynamo, we will start with presenting the works related to the re-commissioning of the Riga dynamo.

2.1. Riga dynamo experiment

On 11 November 1999 the kinematic phase of magnetic-field self-excitation was shortly observed at the Riga dynamo facility before the experiment had to be stopped due to a minor leakage of liquid sodium [9]. After some repairs, in July 2000, a number of full runs clearly demonstrated both the kinematic and the saturated dynamo regime [10], thereby laying the basis for a comprehensive data base including growth rates, frequencies, and spatial structures of the magnetic eigenfield in dependence on the impeller's rotation rate [38]. Data of the kinematic regime was shown to be in very good agreement with numerical predictions [45], and even the saturation regime was reasonably understood by applying Lenz's rule to the specifics of this hydrodynamic dynamo [46].

After a series of experimental campaigns, which delivered quite reliable and reproducible results, the Riga dynamo was disassembled in order to replace and stabilize an inner cylinder that had been deformed during one run in 2010. The project A2 supported the refurbishment with the double aim of testing measurement techniques for the DRESDYN precession dynamo, and of preparing such a modification of the experiment that allows for observing new and non-trivial back-reaction effects.

The latter was motivated by the numerical finding that a specific "de-optimization" of the flow field in the Riga dynamo could lead to a vacillation between two different states of the dynamo [47]. Actually, we set out from the hypothesis that a too high initial azimuthal component of the velocity might yield a subcritical Hopf bifurcation, just by virtue of a selective breaking of this component that provides a "re-optimization" of the velocity. Instead of such a "hard" subcritical Hopf bifurcation we found numerically a "soft" vacillation between two dynamo states with different kinetic and magnetic energies. For still larger magnetic Reynolds numbers even a transition to chaos was predicted.

Based on these findings, one of the tasks of the A2 project was to figure out how such scenarios could be realized in the Riga dynamo facility. We evaluated several technical provisions to increase the azimuthal velocity component beyond its optimal value, without completely destroying the flow structure that had been carefully optimized for the original Riga dynamo [45]. A hydraulic analysis provided some feasible shapes and pitch angles of the post-propeller vanes that indeed should produce the desired azimuthal velocities. Figure 2a shows the resulting geometries and the corresponding velocity profile. However, before implementing this new vanes' configuration we decided to first re-assemble the Riga dynamo in its old form (with a stabilized second cylinder in order to prevent buckling) and to validate reproducibility of the former

dynamo . Figure 2b shows the self-excited magnetic field at different radial positions within the dynamo as observed in the first experimental campaign after re-commissioning in June 2016. More details can be found in [48].

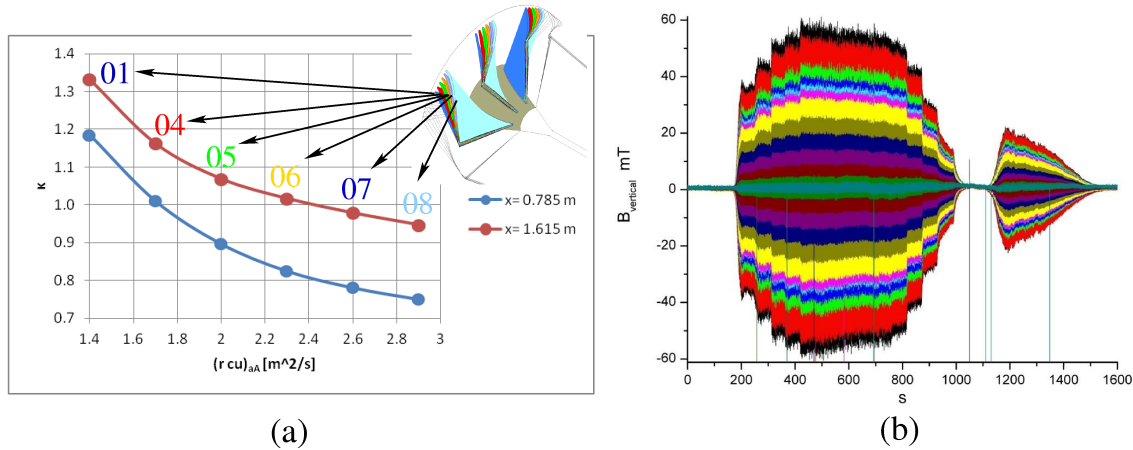


Figure 2. Riga dynamo experiment. (a) Targeted "de-optimization" of the flow profile behind the impeller by choosing vanes with increasing pitch angles. The curves show the ratio $\kappa = \sqrt{\bar{v}_z^2 / (2\bar{v}_\phi^2)}$ of mean axial to mean azimuthal velocity, in dependence on the swirl of the flow, for various vanes and two distances x from the impeller. (b) Vertical magnetic field measured at different radial position in the first run after recommissioning (June 2016).

While the data are still under detailed analysis, we can conclude that the Riga dynamo experiment is now available for research into non-trivial back-reaction effects, and for testing measurement techniques for the DRESHDYN precession dynamo.

2.2. Numerical and experimental results on precession-driven flows in cylinders

The largest installation in the framework of DRESHDYN is a precession-driven liquid sodium experiment. Guided by early numerical estimations of the dynamo threshold of precession driven flows in cylinders [49, 37, 50] and cubes [51], a magnetic Reynolds number of $Rm \approx 700$ was striven for. This ambitious number is achieved with a cylinder diameter of 2 m rotating at 10 Hz.

Design and construction of the precession dynamo experiment (see Figure 3) is the responsibility of SBS Bühnentechnik GmbH. A detailed shape optimization of the rotating vessel turned out to be necessary in order to cope with the huge stresses that result during precessing. The facility is presently under construction, and first pre-experiments with water are expected for late 2018.

In preparing this large-scale experiment, a 1:6 scaled water experiment (see Figure 4a) was built and utilized in order to gain insight into the flow structure and the pressure field for varying Reynolds numbers and precession ratios (Poincaré numbers). Parallel to that, the spectral element code SEMTEX [52] was qualified and intensely used for precession-driven flows in cylinders. While such simulations are restricted to Reynolds numbers of about $Re = 10^4$, the large experiment will reach approximately 10^8 . The 1:6 water experiment reaches a number of 1.6×10^6 when run at 10 Hz, but can also be slowed down to reach a value of 10^4 , thereby guaranteeing some overlap with numerical simulations.

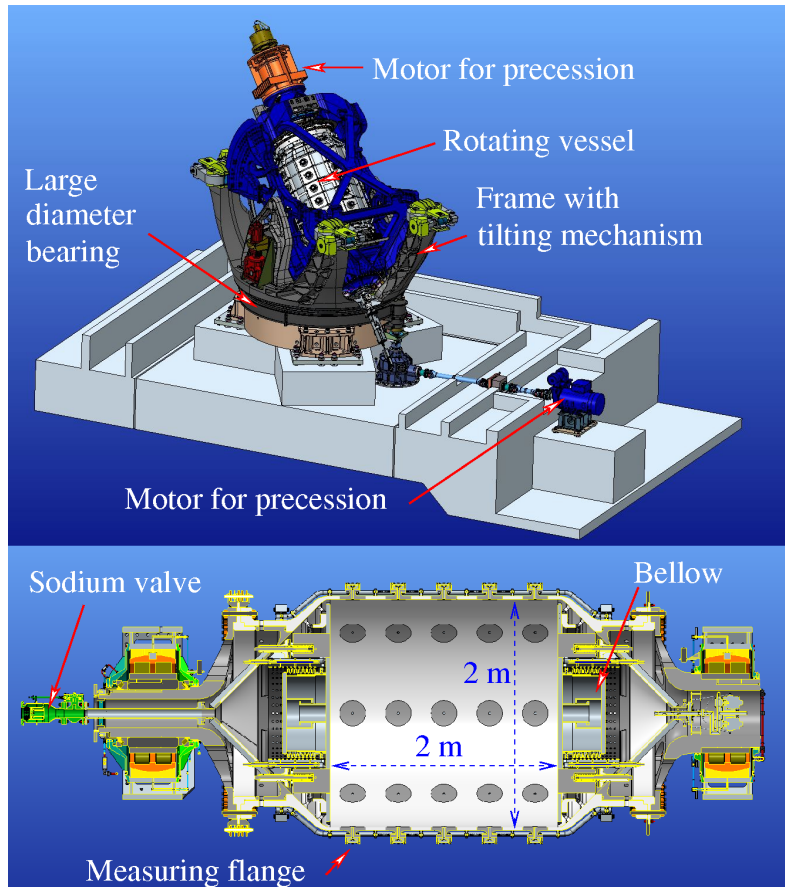


Figure 3. Design of the precession-driven dynamo experiment. Figure courtesy SBS Bühnentechnik GmbH.

A significant share of simulations and experiments was invested into estimating the pressure field, a crucial input for the (static and dynamic) strength evaluation of the vessel. While pure rotation with 10 Hz leads already to a centrifugal pressure of about 20 bar, it is the precession-driven pressure pulsation on the order of 10 bar that makes the (dynamic) strength validation so challenging.

Figure 4 illustrates the flow structure (c,d,e) and the corresponding pressure field (f,g,h) computed at $Re = 6500$ and a Poincaré number $Po \equiv \Omega_{\text{precession}}/\Omega_{\text{rotation}} = 0.02$ for three angles between the rotation axis and the precession axis 45° , 90° , and 135° . The maximum pressure pulsations in dependence on Po are shown in Figure 4b, together with the corresponding values resulting from the small water experiment (note that all values are up-scaled to the conditions of the large experiment). Basically, at low Po the flow is dominated by the first ($m = 1$) Kelvin mode which is mirrored also by the increasing pressure pulsation. Approximately at $Po = 0.03$, higher azimuthal modes become relevant by drawing more and more energy from the forced $m = 1$ Kelvin mode. The curve's kink at $Po = 0.07$ indicates a sudden transition of this quasi-laminar regime to a turbulent regime, which is also confirmed by the hysteretic behaviour of the motor power at this point [53]. The obvious difference between the simulated and experimental curves is quite telling: transition to turbulence is strongly delayed in the (still highly viscous) numerical case which also shows significantly higher pressure pulsations.

Apart from this rather global feature, our numerical simulation have also characterized the

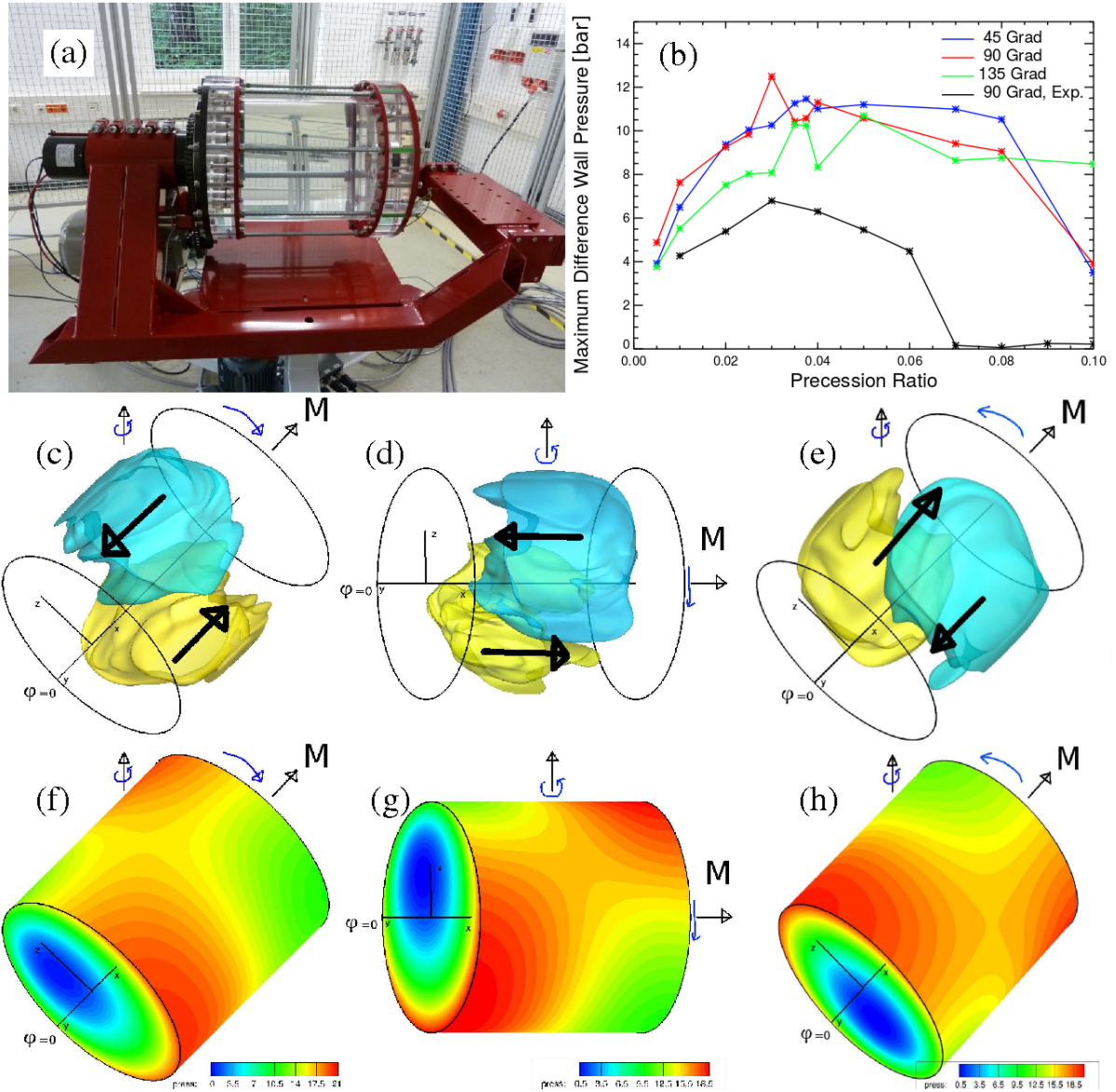


Figure 4. Experimental and numerical preparations for the large precession experiment. (a) 1:6 down-scaled water experiment. (b) Maximum pressure difference at the wall. The numerical curves, computed at $Re = 6500$, are for the three different precession angles 45° (blue), 90° (red), and 135° (green). The black curve gives the experimental data for 90° measured at $Re = 1.6 \times 10^6$. The middle row shows the numerically simulated axial velocity component for the angles 45° (c), 90° (d), and 135° (e), the lower row (f,g,h) the corresponding pressure fields.

onset of higher m -modes which usually are excited by triadic resonances with the forced $m = 1$ Kelvin modes [54].

2.3. Precession-driven dynamos in cylinders and cubes

Dynamo action of precession-driven flows is, unfortunately, a largely unsolved problem, despite a number of attempts to apply it to the dynamo of the Earth and other cosmic bodies [55, 56, 57, 58, 59]. The DRESYDYN precession dynamo experiment was partly motivated by the

optimistic numerical estimations obtained by Nore [49, 37] for the cylinder, and Krauze [51] for a cube; both pointed consistently to a critical Rm on the order of 700.

Unfortunately, this optimistic value is challenged when going to smaller values of the magnetic Prandtl number [61], i.e. to higher Reynolds numbers. Here, even the structure of the hydrodynamic flow, and its dependence on the precession ratio and the tilt angle, is largely unknown. Recent simulations and experiments have revealed the occurrence of higher m -modes [60, 54] whose dynamo capabilities are still under scrutiny. Even less is known about the turbulent flow structure when crossing the critical precession ratio.

Typically, direct numerical simulations for precessing flows with correct no-slip boundary conditions work only until $Re \approx 10^4$. A promising way of going to much larger values of Re is to replace no-slip boundary conditions by stress-free conditions, thereby avoiding the need to resolve the viscous boundary layer. Such an approach was pursued by Goepfert and Tilgner [62] who studied a precessing flow, and its dynamo action, in a cube. While this is by no means an astrophysically relevant geometry, one may naively expect the flow in a cube to resemble the flow in the largest sphere enclosed by the cube, with some dead water concentrated in the corners. The main hope is that there are some features common to precessing flows in all geometries, such as the appearance of triadic resonances, so that any geometry is useful as a model system.

The dynamo action of this flow depends quite sensitively, partly erratically, on the Reynolds and the Poincare numbers. Figure 5 illustrates the flow and the self-excited magnetic field for two different parameter sets.

3. Magnetically triggered flow instabilities

We turn now to the field of magnetically triggered flow instabilities, and report the main experimental and theoretical results obtained within project A2.

3.1. Experimental demonstration of AMRI, and the large MRI/TI experiment

After HMRI [22, 24] (and TI [30]) had been experimentally demonstrated prior to the start of the LIMTECH Alliance, the PROMISE facility was qualified for the experimental investigation of AMRI [31]. Since AMRI needs a minimum central current of about 10 kA (given the material parameters of GaInSn) the power supply for this current had to be enhanced to deliver 20 kA.

Figure 6 illustrates the dependence of various numerically and experimentally obtained quantities on the central current (or the Hartmann number). Figure 6a shows the growth rate obtained with a 1D stability code, for $Re = 1480$, whose positive segment indicates the existence of AMRI in an interval approximately between 10 and 22 kA. Quite in correspondence with that, the lowermost curve ("Sim: ideal B") in Figure 6b shows the expected rms value of the axial velocity, under the assumption of a purely azimuthal applied magnetic field. But here is a subtlety: The curve with the highest values ("Sim: real B") in Figure 6b gives the corresponding numerical rms values for the case that the real magnetic field of the experimental setting is assumed. This field deviates slightly from a pure B_ϕ , since the two leads from and to the power supply form a single-winding coil. Although the resulting deviation of the field is only in the region of a few per cent, the rms values are significantly enhanced, and show also a broadened range for AMRI. Interestingly, the experimental curve ("Experiment") shows a very similar shape, albeit with somewhat lower values.

The explanation of this phenomenon needs some peculiar symmetry considerations: Let us start with an infinitely long TC flow under the influence of a purely azimuthal magnetic field. As known from [25], this configuration has no preference for $m = 1$ or $m = -1$ modes, so that both together would be expected to form a standing wave. In a finite length TC cell, the Ekman pumping at the lids produces slight deviations from the perfect TC flow, which leads to some preference for either $m = 1$ or $m = -1$ modes in the upper and lower halves (see the simulation in Figure 6d). Adding now a second type of symmetry breaking, in form of an

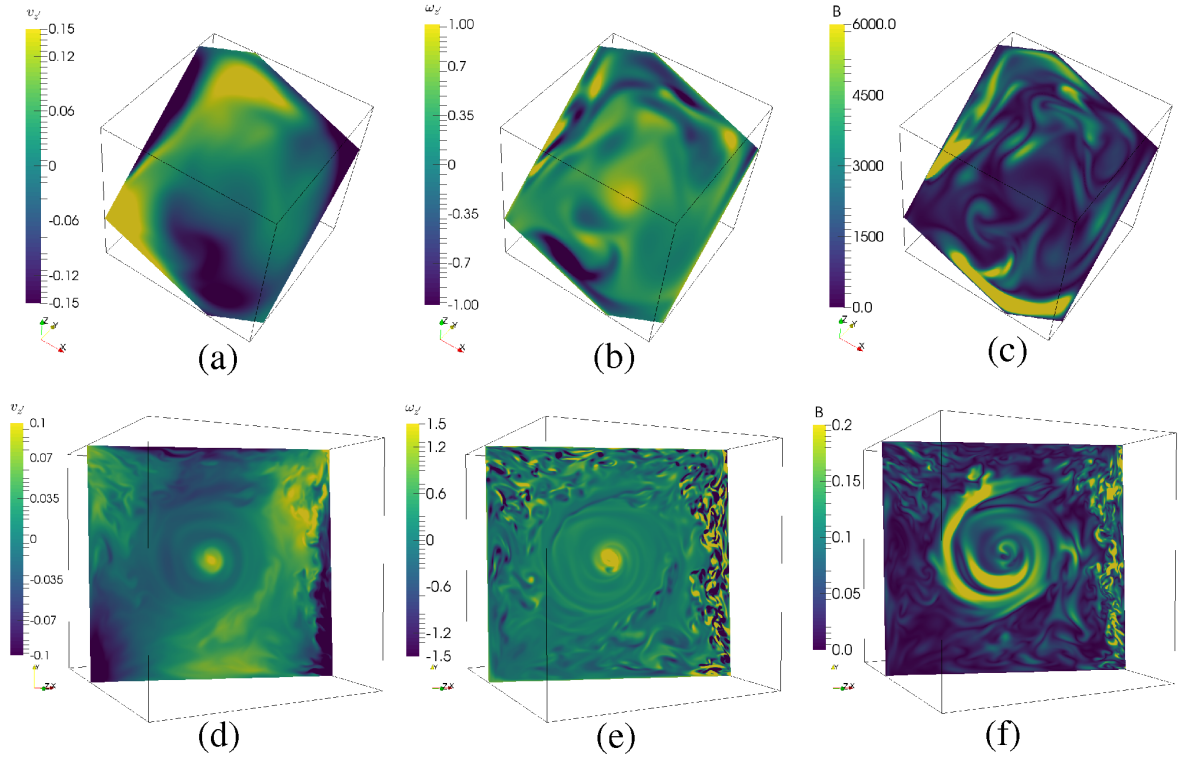


Figure 5. Two different kinds of dynamos in a precessing cube. Upper row: $Re = 4 \times 10^3$, $\overline{Po} = -0.16$. Lower row: $Re = 10^5$, $\overline{Po} = -0.02$. (Note the somewhat different definition of the Poincare number used here: $\overline{Po} = Po/(1 + Po \cos \alpha)$, with α denoting the precession angle). Visualization of the velocity component parallel to the rotation axis of the fluid (a,d), of the total vorticity (b,e), and of the magnitude of the magnetic field (c,f) in the plane perpendicular to this rotation axis.

imperfect applied magnetic field, the original $m = \pm 1$ symmetry of the instability is to some extent restored. In other words, the upward and downward travelling modes that would be expected to be concentrated in the upper and lower part, now interpenetrate each other (see simulation in Figure 6e) and populate now also the mid-height region, which effectively results in significantly enhanced rms values. This behaviour is indeed found in the experiment (Figure 6f).

While this simulated, and experimentally confirmed, effect of a double symmetry breaking on the AMRI is interesting in its own right, we have decided to improve the PROMISE facility in such a way that the azimuthal symmetry breaking is largely preserved. This is realized by a new system of wiring of the central current, comprising now a "pentagon" of 5 back-wires situated around the experiment. First experiments with this set-up show encouraging results, in particular transitions between AMRI and HMRI when adding an axial field to the azimuthal one.

The second large-scale sodium experiment to be set-up within the DRESHDYN project aims at investigating combinations of different versions of the MRI and the current-driven TI (see Figure 7). Basically, the set-up is designed as a TC experiment with 2 m fluid height, an inner radius $r_{in} = 20$ cm and an outer radius $r_{out} = 40$ cm. Rotating the inner cylinder at up to 20 Hz, we plan to reach $Rm \sim 40$, while the planned axial magnetic field $B_z = 120$ mT will correspond to a Lundquist number $S := Pm^{1/2}Ha \sim 8$. Both values are about twice the respective critical

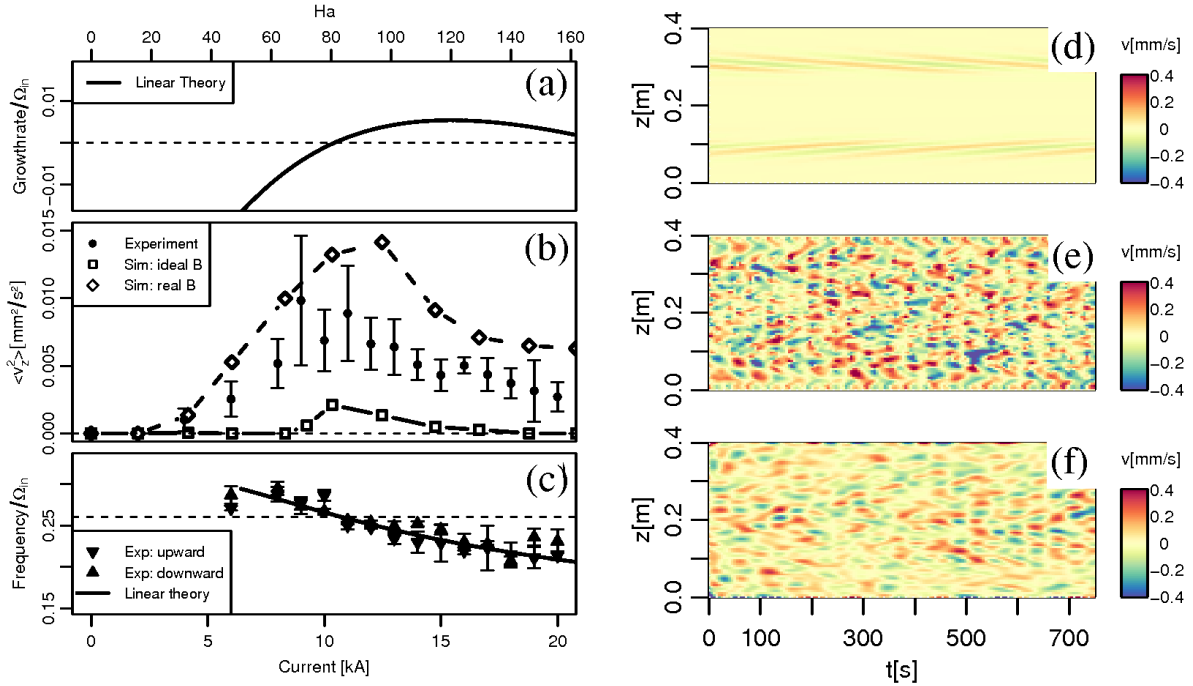


Figure 6. Results of the AMRI experiment. Left: Dependence of various quantities on Ha. (a) Numerically determined growth rate. (b) Mean squared velocity perturbation. (c) Angular drift frequency. In the frequency plot, “upward” and “downward” refer to the travel direction of the AMRI wave. Right: Velocity perturbation $v_z(m = 1, z, t)$ for $\mu := \Omega_{\text{out}}/\Omega_{\text{in}} = 0.26$, $\text{Re} = 1480$, and $\text{Ha} = 124$. (d) Simulation for ideal axisymmetric field. (e) Simulation for realistic field. (f) Experimental results. After [31].

values for the onset of SMRI as they were derived in [64].

Below those critical values, we plan to investigate how HMRI approaches the limit of SMRI [20, 21]. To this end, we will use a strong central current, as it is already present in the PROMISE experiment [24, 31]. This insulated central current can be supplemented by another axial current guided through the (rotating) liquid sodium, which will further allow to investigate combinations of MRI and TI. Theoretical studies [65, 67, 68, 69] have shown that even a slight addition of current through the liquid extends the range of application of the helical and azimuthal MRI to Keplerian flow profiles.

3.2. Between HMRI, AMRI and TI: Some theoretical results

Shortly after the numerical revelation of HMRI by Hollerbach and Rüdiger [20], Liu et al. [71] had derived – in the framework of a short-wavelength (or WKB) approximation – two limits for the negative and positive shear between which HMRI should cease to exist. Expressed in terms of the Rossby number $\text{Ro} \equiv r/(2\Omega)\partial\Omega/\partial r$, the lower Liu limit (LLL) $\text{Ro}_{\text{LLL}} = 2(1 - \sqrt{2}) \approx -0.828$ has attracted a lot of interest [72, 73], in particular since it would prevent HMRI from working for astrophysically interesting Keplerian flows characterized by $\text{Ro}_{\text{Kepler}} = -0.75$. In contrast to this, the upper Liu limit $\text{Ro}_{\text{ULL}} = 2(1 + \sqrt{2}) \approx 4.828$ for positive shear flows has been largely ignored, although positive shear flows are indeed relevant in astrophysics, for example in a $\pm 30^\circ$ strip of the solar tachocline. We note in passing that positive shear flows were usually considered perfectly stable (even under the action of vertical magnetic fields), so that Deguchi’s

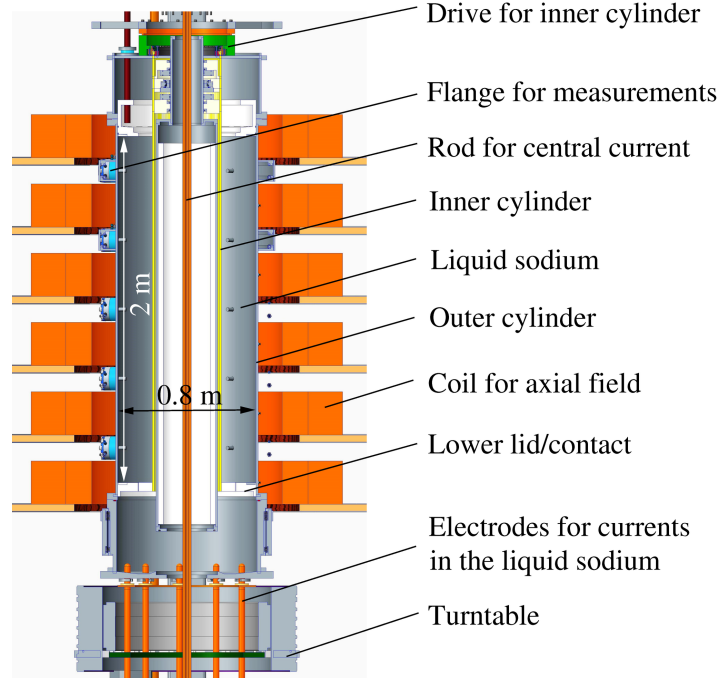


Figure 7. Design of the large-scale TC experiment for investigations of HMRI, AMRI, SMRI, TI and their combinations.

recent discovery of a linear instability for very large Reynolds numbers came as a big surprise [74].

A first interesting result regarding the two Liu limits was published in [65]. This work dealt with the question how HMRI (and AMRI) would be modified if the central current, which generates the azimuthal field component, was gradually complemented by some second axial current through the liquid. The respective weight of the two azimuthal field parts can be quantified by the magnetic Rossby number $Rb \equiv r^2/(2B_\phi)\partial(r^{-1}B_\phi)/\partial r$ which is constructed as a counterpart of Ro . A pure current-free field (as assumed for HMRI and AMRI [66]) gives $Rb = -1$, while a pure current in the fluid (as for TI) corresponds to $Rb = 0$. In [65], and more detailed in [67], it was shown that the LLL and the ULL are just the endpoints of one common stability curve (Figure 8) in the $Ro - Rb$ plane which acquires the surprisingly simple analytical form

$$Rb = -\frac{1}{8} \frac{(Ro + 2)^2}{Ro + 1}, \quad (1)$$

when both Re and Ha are sent to infinity and either the ratio of azimuthal to axial field (for HMRI) or the shape of the perturbation (for AMRI) is optimized. The "metamorphosis" of the helical MRI when changing the ratio of the axial currents within the fluid and on the axis were also studied with a 1D stability code [68].

The treatment of problems with variable Rb led also to the reconsideration of an old problem of magnetohydrodynamics which is known as Chandrasekhar's theorem [75]. In the framework of ideal MHD this theorem states the stability of rotating flows of any radial dependence under the influence of an azimuthal magnetic field whose corresponding Alfvén velocity has the same amplitude and radial dependence as the rotation. Both in the WKB framework [67] and with a 1D-stability code [69] we showed that these Chandrasekhar solutions can be destabilized in non-ideal MHD.

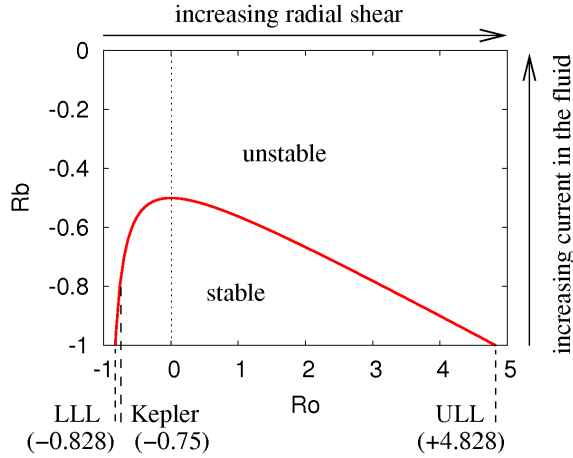


Figure 8. Stability chart in the $Ro - Rb$ plane, for $Pm = 0$ and Ha and Re tending to infinity. The Liu limits LLL and ULL apply only for $Rb = -1$, while for $Rb > -1$ shallower shear profiles can as well be destabilized (including Kepler rotation with $Ro = -0.75$, starting at $Rb = -0.78125$). The dotted line separates flows with negative shear (to the left) and positive shear (to the right).

We also mention the paper by Priede [70] that, treating a simplified pinch-type instability in a semi-infinite planar sheet of an inviscid incompressible liquid with a straight rigid edge, helped to clarify some differences between the instability mechanisms in highly resistive and well conducting fluids, resulting in different development times: magnetic response time for the former, and the much shorter Alfvén time for the latter.

3.3. Super-AMRI

Within the project, we have proved the existence of the upper Liu limit also for purely azimuthal magnetic fields, both in WKB approximation [76] and with a 1D stability code [77, 78]. The seed grant "Super-AMRI" was dedicated to find optimal parameters for a liquid metal TC experiment to show this "Super-AMRI", as we call it now. The main problem here is that such a TC experiment would need a rather thin gap in order to realize the enormous positive shear of $Ro > 4.828$, which leads to a very large critical value of the central current. For a liquid sodium experiment, both WKB [76] and 1D simulations with insulating boundary conditions [78] point to a critical current of about 80 kA, while a much lower (and experimentally more feasible) value of some 20 kA results for ideally conducting cylinder walls [78]. Figure 9 shows the stability maps in the Hartmann-Reynolds plane for $r_{in}/r_{out} = 0.75$ (a) and $r_{in}/r_{out} = 0.9$ (b) and two magnetic Prandtl numbers 10^{-5} (red) and 10^{-2} (blue), without (AMRI) and with (TI) current in the fluid, together with the simulated axial velocity component (c) for the case $r_{in}/r_{out} = 0.75$. The technically feasible combination of using sodium and copper walls is expected to lead to a critical current between 20 kA and 80 kA, but a detailed simulation for that case is still in progress.

Hence, it might be worthwhile to come back to the idea of "Super-HMRI", for which a 1D simulation is also pending. With view on the significant differences in the axial currents that are needed for the experimental observation of the negative-shear versions of HMRI (4 kA) and AMRI (10 kA), we expect a similar reduction in the positive shear case that could reduce the technical efforts significantly.

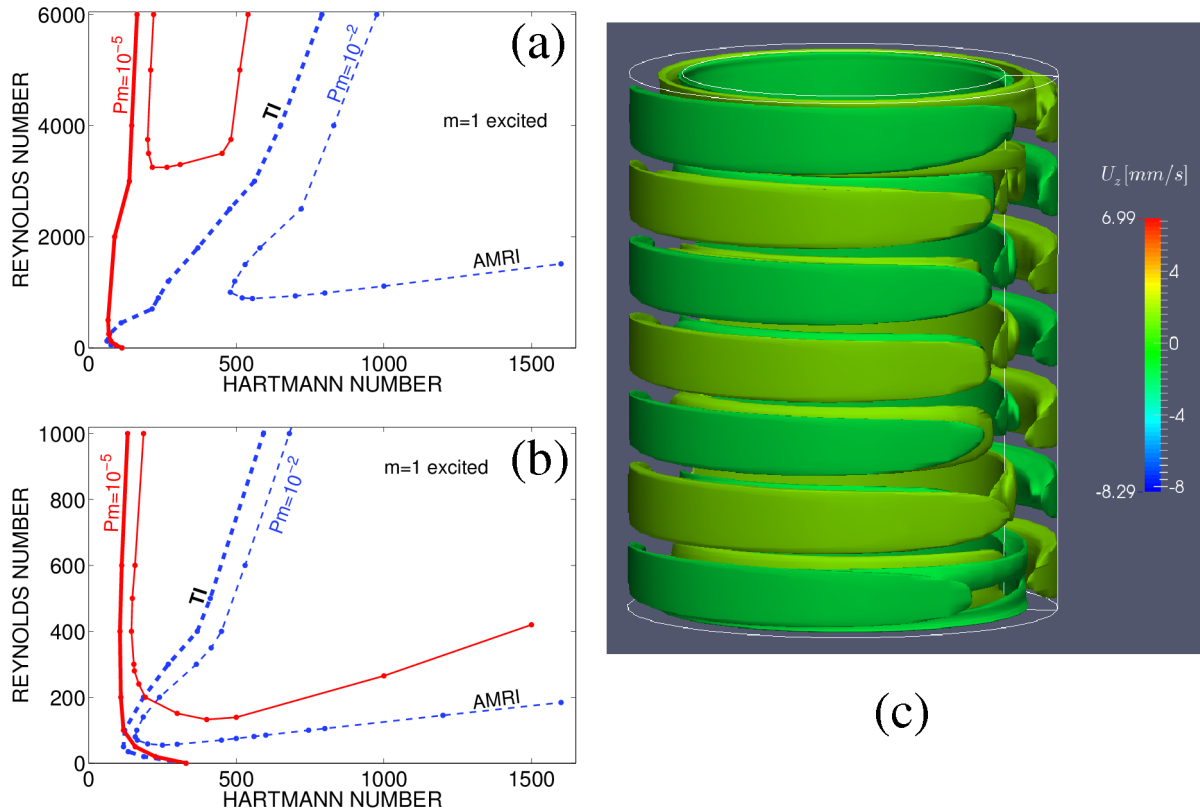


Figure 9. Azimuthal MRI for flows with positive shear (Super-AMRI): (a) Stability maps in the Hartmann-Reynolds plane for resting inner cylinder with $r_{in}/r_{out} = 0.75$ and two magnetic Prandtl numbers 10^{-5} (red) and 10^{-2} (blue), without (AMRI) and with (TI) current in the fluid. (b) The same for $r_{in}/r_{out} = 0.9$. (c) Simulated axial velocity component for $r_{in}/r_{out} = 0.75$.

3.4. Linking dissipation-induced instabilities and non-modal growth

While the two Liu limits for HMRI have been known for more than a decade [71], the physical reason behind them was never brought into question. In a recent paper [79], we have revealed a link between the modal growth *rate* of HMRI (from which the Liu limits follow) and the non-modal growth *factor* of the underlying purely hydrodynamical problem, which sheds some new light on the physical essence of both.

Non-modal (or transient) growth is typical for the time evolution of dynamical systems governed by non-normal operators. Due to the non-orthogonality of their eigenfunctions, an appropriately chosen initial state can experience a transient growth of its amplitude even if the (two or more) individual eigenfunctions of which it is composed have negative modal growth rates. Non-modal instabilities are known to play a key role in explaining the onset of turbulence in pipe flows [80].

As shown by Afshordy et al. [81], the non-modal growth factor for axisymmetric perturbations of purely hydrodynamic rotating flows can be expressed by the surprisingly simple equation $G = (1 + Ro)^{sgn(Ro)}$ which is illustrated by the red curve in Figure 10. Comparing this with the equation for the modal growth rate γ (green curve in Figure 10) of HMRI [67], we find the

following link [79]:

$$\gamma = \frac{\text{Ha}^2}{\text{Re}} \left[\frac{(\text{Ro} + 2)^2}{8(\text{Ro} + 1)} - 1 \right] = \frac{\text{Ha}^2}{\text{Re}} \left[\frac{(G + 1)^2}{8G} - 1 \right]. \quad (2)$$

For large $|\text{Ro}|$ this leads to a simple linear relation of γ and G : $\gamma \approx \text{Ha}^2/\text{Re}(G/8 - 3/4)$. Figure 10 illustrates this asymptotic connection. At the two Liu limits of HMRI, $\text{Ro} = 2(1 \pm \sqrt{2})$, G acquires the same value $G = 1 + 2(1 + \sqrt{2}) \approx 5.828$.

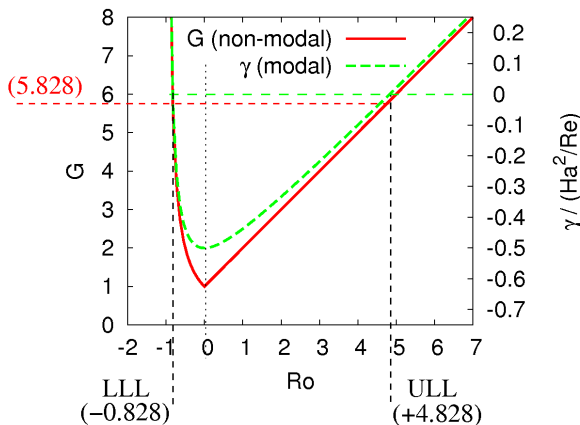


Figure 10. Non-modal growth factor G for purely hydrodynamic rotating flows (red curve), and normalized growth rate γ of helical MRI (green curve), in dependence on the Rossby number Ro . The two quantities are connected by Equation (2) and match asymptotically according to $\gamma \approx \text{Ha}^2/\text{Re}(G/8 - 3/4)$.

Keeping in mind that HMRI is a (double-)diffusive instability, we learn that it is inherently based on the non-modal growth of the underlying purely hydrodynamic flow. For a linear instability to become effective, it requires some dissipation to allow a coupling between different components of the eigenfunctions (actually between meridional and azimuthal flow perturbations, as shown in [82]). Once this coupling is established, the growth rate of the linear HMRI becomes (nearly) proportional to the non-modal growth factor of the underlying hydrodynamic flow.

It remains to be seen whether similar links exist also in other fields of hydrodynamics. This is not obvious, as we have already experienced when analyzing the corresponding connection for AMRI [83] that is more subtle due to the shear-induced time-variation of the wavenumber of the $m = 1$ mode.

4. Conclusions

Two large-scale liquid sodium experiments, on precession and on MRI/TI, are presently under construction at HZDR. For both of them, the project A2 of the LIMTECH Alliance has made theoretical and experimental contributions. The project has further supported re-commissioning of the Riga dynamo experiment which is now ready for studying new interesting back-reaction effects as well as for testing measurement techniques for the DRESHDYN experiments. A particular achievement of the project is a deepened insight into the diffusive instabilities of rotating flows under the action of magnetic fields. As an outcome of those activities, the starting grant on "Super-AMRI" has delivered first parameter estimates for a new liquid sodium

experiment on the magnetic destabilization of positive shear flows. Another result concerns the rigorous mathematical link between the non-normal growth factor of purely hydrodynamic rotating flows with the normal growth rate of the HMRI which gives – to the best of our knowledge – the first link between non-normal growth and diffusive (or dissipation-induced) instabilities. We should also mention here the recent astrophysical application of AMRI for explaining the angular momentum redistribution of post-main sequence low-mass stars [84].

Many problems related to the TI liquid metals were investigated in close collaboration with the project B3 which was dedicated to applied problems of liquid metal batteries [85, 86, 87]. As one of the potentially dangerous instabilities, which would occur even if electrovortex flows and sloshing instabilities were completely suppressed, the TI was numerically treated with an OpenFOAM code enhanced by a Poisson solver for the electric potential and Biot-Savart’s law for the induced magnetic field [85]. With this code it was possible to test various provisions for suppressing the TI and to understand its saturation mechanism [86]. An interesting by-product of these simulations was the detection of helicity oscillations [88] for small magnetic Prandtl numbers. Re-applying this result (obtained for liquid metal batteries) to a simple model of a Tayler-Spruit solar dynamo, we identified a mechanism that could empower the weak tidal forces of planets to synchronize the Hale cycle of the solar magnetic field [89, 90]. It is here where the synergies between basic research and liquid metal technologies, which were fostered by the LIMTECH Alliance, proved particularly useful.

Acknowledgments

This work was supported by Helmholtz-Gemeinschaft in frame of the LIMTECH Alliance. Close cooperation with Tom Weier and Norbert Weber (project B3) on various aspects of the Tayler instability is gratefully acknowledged.

- [1] Jones C 2011 *Annu. Rev. Fluid Mech.* **43** 583
- [2] Charbonneau P 2014 *Annu. Rev. Astron. Astrophys.* **52** 251
- [3] Beck R 2009 *Astrophys. Space Sci. Trans.* **5** 43
- [4] Balbus S A 2003 *Ann. Rev. Astron. Astrophys.* **41** 555
- [5] Tayler R J 1973 *Mon. Not. R. Acad. Sci.* **161** 365
- [6] Gailitis A, Lielausis O, Platacis E, Gerbeth G and Stefani F 2002 *Rev. Mod. Phys.* **74** 973
- [7] Stefani F, Gailitis A and Gerbeth G 2008 *ZAMM* **88** 930
- [8] Lathrop D P and Forest C B 2011 *Phys. Today* **64** 40
- [9] Gailitis A et al. 2000 *Phys. Rev. Lett.* **84** 4365
- [10] Gailitis A et al. 2001 *Phys. Rev. Lett.* **86** 3024
- [11] Stieglitz R and Müller U 2000 *Phys. Fluids*. **13** 561
- [12] Berhanu M et al 2010 *Eur. Phys. J. B* **77** 459
- [13] Stefani F, Gerbeth G, Günther U and Xu M 2006 *Earth Planet. Sci. Lett.* **243** 828
- [14] Sorriso-Valvo L, Stefani F, Carbone V, Nigro G, Lepreti F, Vecchio A and Veltri P 2007 *Phys. Earth Planet. Int.* **164** 197
- [15] Petrelis F, Fauve S and Dormy E 2009 *Phys. Rev. Lett.* **102** 144503
- [16] Benzi R and Pinton J F 2010 *Phys. Rev. Lett.* **105** 024501
- [17] Sisan D et al 2004 *Phys. Rev. Lett.* **93** 114502
- [18] Nornberg M D, Ji H, Scharfman E, Roach A and Goodman J 2010 *Phys. Rev. Lett.* **104** 074501
- [19] Roach A H, Spence E J, Gissinger C, Edlund E M, Sloboda P, Goodman J and Ji H 2012 *Phys. Rev. Lett.* **108** 154502
- [20] Hollerbach R and Rüdiger G 2005 *Phys. Rev. Lett.* **95** 124501
- [21] Kirillov O N and Stefani F 2010 *Astrophys. J.* **712** 52
- [22] Stefani F, Gundrum T, Gerbeth G, Rüdiger G, Schultz M, Szklarski J and Hollerbach R 2006 *Phys. Rev. Lett.* **97** 184502
- [23] Stefani F, Gundrum T, Gerbeth G, Rüdiger G, Szklarski J and Hollerbach R 2007 *New J. Phys.* **9** 295
- [24] Stefani F, Gerbeth G, Gundrum T, Hollerbach R, Priede J, Rüdiger G and Szklarski J 2009 *Phys. Rev. E* **80** 066303
- [25] Hollerbach R, Teeluck V and Rüdiger G 2010 *Phys. Rev. Lett.* **104** 044502

- [26] Bergerson W F, Hannum D A, Hegna C C, Kendrick R D, Sarff J S and Forest C B 2006 *Phys. Rev. Lett.* **96** 015004
- [27] Spruit H C 2002 *Astron. Astrophys.* **381** 923
- [28] Gellert M, Rüdiger G and Elstner D 2008 *Astron. Astrophys.* **479** L33
- [29] Rüdiger G, Schultz M and Gellert M 2011 *Astron. Nachr.* **332** 17
- [30] Seilmayer M et al 2012 *Phys. Rev. Lett.* **108** 244501
- [31] Seilmayer M et al 2014 *Phys. Rev. Lett.* **113** 024505
- [32] Zimmermann D S, Triana S A, Nataf H-C and Lathrop D P 2010 *J. Geophys. Res. - Sol. Earth* **119** 4538
- [33] Adams M M, Stone D R, Zimmerman D S and Lathrop D P 2015 *Prog. Earth Planet. Sci.* **29** 1
- [34] Cooper C M et al. 2014 *Phys. Plasmas* **21** 013505
- [35] Weisberg D B, Peterson E, Milhone J, Endrizzi D, Cooper C, Désangles V, Khalzov I, Siller R and Forest C B *Phys. Plasmas* **24** 056502
- [36] Stefani F, Eckert S, Gerbeth G, Giesecke A, Gundrum T, Steglich C, Weier T and Wustmann B 2012 *Magnetohydrodynamics* **48** 103
- [37] Stefani F, Albrecht T, Gerbeth G, Giesecke A, Gundrum T, Herault J, Nore C and Steglich C 2015 *Magnetohydrodynamics* **51** 275
- [38] Gailitis A, Gerbeth G, Gundrum T, Lielausis O, Platacis E and Stefani F *Comptes R. Phys.* **9** 721
- [39] Tilgner A and Busse F H 2001 *Saturation mechanism in a model of the Karlsruhe dynamo* (Dynamo and Dynamics: A mathematic challenge) ed P Chossat, D Armbruster, I Oprea (Dordrecht: Springer) pp 109-116
- [40] Rädler K-H and Brandenburg A 2003 *Phys. Rev. E* **67** 026401
- [41] Giesecke A, Stefani F and Gerbeth G 2010 *Phys. Rev. Lett.* **104** 044503
- [42] Giesecke A, Nore C, Stefani F, Gerbeth G, Léorat J, Herreman W, and Guermond J-L 2012 *New. J. Phys.* **14** 053005
- [43] Nore C, Léorat J, Guermond J-L, 2015 *Phys. Rev. E* **91** 013008
- [44] Nore C, Quiroz D C, Cappanera L, Guermond J-L 2016 *Europhys. Lett.* **114** 65002
- [45] Stefani F, Gerbeth G and Gailitis A 1999 *Velocity profile optimization for the Riga dynamo experiment* (Transfer phenomena in magnetohydrodynamic and electroconducting flows) ed A Alemany, Ph Marty, J-P Marty (Dordrecht: Kluwer) pp 31-44
- [46] Gailitis A, Lielausis O, Platacis E, Gerbeth G and Stefani F 2004 *Phys. Plasmas* **11** 2838
- [47] Stefani F, Gailitis A and Gerbeth G 2011 *Astron. Nachr.* **332** 4
- [48] Gailitis A and Lipsbergs G 2017 *Magnetohydrodynamics* in press
- [49] Nore C, Léorat L, Guermond J-L and Luddens F 2011 *Phys. Rev. E* **84** 016317
- [50] Cappanera L, Guermond J-L, Léorat and Nore C 2016 *Phys. Rev. E* **93** 043113
- [51] Krauze A 2010 *Magnetohydrodynamics* **46** 271
- [52] Blackburn H M and Sherwin S J (2004) *J. Comp. Phys.* **197** 759
- [53] Herault J, Gundrum T, Giesecke A and Stefani F 2015 *Phys. Fluids* **27** 124102
- [54] Giesecke A, Albrecht T, Gundrum T, Herault J and Stefani F 2015 *New J. Phys.* **17** 113044
- [55] Malkus W V R 1968 *Science* **160** 259
- [56] Vanyo J P 2004 *Geophys. J. Int.* **158** 470
- [57] Tilgner A 2005 *Phys. Fluids* **17** 034104
- [58] Dwyer C A, Stevenson D J and Nimmo F 2011 *Nature* **479** 212
- [59] Fu R R et al 2012 *Science* **338** 238
- [60] Albrecht T, Blackburn H M, Lopez J M, Manasseh R and Meunier P 2015 *J Fluid Mech.* **778** R1
- [61] Giesecke A, Albrecht T, Gerbeth G, Gundrum G and Stefani F 2015 *Magnetohydrodynamics* **51** 293
- [62] Goepfert O and Tilgner A 2016 *New J. Phys.* **18** 103019
- [63] Gans R 1970 *J. Fluid Mech.* **45** 111
- [64] Rüdiger G and Shalybkov D 2003 *Phys. Rev. E* **67** 046312
- [65] Kirillov O N and Stefani F 2013 *Phys. Rev. Lett.* **111** 061103
- [66] Kirillov O N and Stefani F and Fukumoto Y 2012 *Astrophys. J.* **756** 83
- [67] Kirillov O N, Stefani F and Fukumoto Y 2014 *J. Fluid Mech.* **760** 591
- [68] Priede J 2015 *Phys. Rev. E* **91** 033014
- [69] Rüdiger G, Schultz M, Stefani F and Mond M 2015 *Astrophys. J.* **811** 84
- [70] Priede J 2017 *J. Fluid Mech.* **816** 705
- [71] Liu W, Goodman J and Ji H 2006 *Astrophys. J.* **643** 306
- [72] Rüdiger G and Hollerbach R *Phys. Rev. E* **76** 068301
- [73] Priede J and Gerbeth G 2009 *Phys. Rev. E* **79** 046310
- [74] Deguchi K 2017 *Phys. Rev. E* **95** 021102(R)
- [75] Chandrasekhar S. 1956 *PNAS* **42** 273

- [76] Stefani F and Kirillov O N 2015 *Phys. Rev E* **92** 051001(R)
- [77] Rüdiger G, Schultz M, Gellert M and Stefani F 2016 *Phys. Fluids* **28** 014105
- [78] Rüdiger G, Gellert M, Schultz M and Stefani F 2016 arXiv:1601.01964
- [79] Mamatsashvili G and Stefani F 2016 *Phys. Rev. E* **94** 051203
- [80] Trefethen A E, Trefethen L N and Schmid P J 1999 *Comput. Methods Appl. Mech. Engrg.* **1926** 413
- [81] Afshordi N, Mukhopadhyay P and Narayan R 2005 *Astrophys. J.* **629** 373
- [82] Priede J, Grants I and Gerbeth G 2007 *Phys. Rev. E* **75** 047303
- [83] Mamatsashvili G and Stefani F 2017 *Magnetohydrodynamics* **53** 107
- [84] Spada F, Gellert M, Arlt R and Deheuvels S 2016 *Astron. Astrophys.* **589** A23
- [85] Weber N, Galindo V, Stefani F, Weier T and Wondrak T 2013 *New J. Phys.* **15** 043034
- [86] Weber N, Galindo V, Stefani F and Weier T 2014 *J. Power Sources* **265** 166
- [87] Weber N, Beckstein P, Herreman W, Horstmann G M, Nore C, Stefani F and Weier T 2017 *Phys. Fluids* **29** 054101
- [88] Weber N, Galindo V, Stefani S, Weier T *New J. Phys.* **17** 113013
- [89] Stefani F, Giesecke A, Weber N and Weier T 2016 *Solar Phys.* **291** 2197
- [90] Stefani F, Galindo A, Giesecke A, Weber N and Weier T 2017 *Magnetohydrodynamics* **53** 169